JOURNAL OF SOLID STATE CHEMISTRY 94, 170–184 (1991)

A New Homologous Series of Lanthanum Copper Oxides

R. J. CAVA, T. SIEGRIST, B. HESSEN, J. J. KRAJEWSKI, W. F. PECK, JR., B. BATLOGG, H. TAKAGI, J. V. WASZCZAK, AND L. F. SCHNEEMEYER

AT&T Bell Laboratories, Murray Hill, New Jersey

AND H. W. ZANDBERGEN

National Centre for High Resolution Electron Microscopy, Delft University of Technology, Delft, Netherlands

Received March 18, 1991; in revised form May 20, 1991

We report the synthesis and structural characterization of a new homologous series of lanthanum cuprates, with the formula $La_{4+4n}Cu_{8+2n}O_{14+8n}$. The $n = 2$ and $n = 3$ members, $La_2Cu_2O_5$ and $La_8Cu_7O_{19}$, synthesized in the bulk, are stable in very narrow temperature ranges in air and oxygen. The $n = 4$ member was observed by electron microscopy. The crystal structure of $La_2Cu_2O_5$ consists of thin ribbons of La_2CuO_4 sandwiched between Cu–O planes of complex low dimensional geometry. The temperature-dependent magnetic susceptibilities of $La_2Cu_2O_5$ and $La_8Cu_7O_{19}$ are characteristic of low dimensional Heisenberg antiferromagnets with a low exchange coupling energy. © 1991 Academic Press, Inc.

The crystal chemistry of perovskite-related copper oxides has recently come to the fore in the search for new high T_c superconductors. The copper oxide-based superconductors are derived from alternating slices of rocksalt and perovskite type structural units (*1, 2*). In many of the superconducting chemical systems, a homologous series of compounds is formed, based on the stacking of different numbers of the rocksalt and perovskite layers. First described for the early transition metal oxides (*3*), the Ruddlesden–Popper series is of the type $A_{n+1}B_nO_{3n+1-\delta}$, where A is the rocksalt layer ion (usually rare earth, alkaline earth, or alkali) and B is the perovskite (transition metal) ion. For copper oxide-based materials, the end members $n = 1$, La_2CuO_4, and the pure perovskite, $n = \infty$, $LaCuO_{3-\delta}$, have been prepared in single-phase form. The former can be synthesized under ambient conditions, but the latter can be prepared only under high oxygen pressures (*4*). The $n = 2$ member is stabilized only by mixing of Sr or Ca on the large atom sites ($La_2SrCu_2O_6$, $La_2CaCu_2O_6$ (*5*)).

Perhaps due to the ubiquity of Ruddelsden–Popper phases in other chemical systems, several groups have claimed to observe them for lanthanum copper oxide, based on the incomplete analysis of X-ray diffraction or electron microscopy data (*6, 7*). Because little (*6*) or no (*7*) synthetic procedure was reported, the results have been widely found to be irreproducible. Here we report that the Ruddelsden–Popper series

0022-4596/91 $3.00

Copyright © 1991 by Academic Press, Inc.
All rights of reproduction in any form reserved.

does *not* occur in the La_2O_3–CuO chemical system under ordinary synthetic conditions, but rather that a homologous series based on a completely different structural principle occurs. Of general formula $La_{4+4n}Cu_{8+2n}O_{14+8n}$, it is based on the insertion of La_2CuO_4 type ribbons of different widths between Cu–O planes of a complex geometry. We report in detail the synthesis, crystal structure, and elementary physical properties of the $n = 2$ member ($La_2Cu_2O_5$), and also information for the $n = 3$ member, $La_8Cu_7O_{19}$. The phases can be synthesized only over very narrow temperature ranges, and will not form if La_2CuO_4 has formed first during the chemical reaction.

Synthesis

Starting materials were high purity La_2O_3 (dried at 900°C in air) and CuO. They were weighed out in appropriate molar proportions and mixed through grinding in a mechanical mortar and pestle for 1 hr. We initially noted the diffraction signature of a new phase for rapidly heated and cooled samples with a $0.5La_2O_3 \cdot 1CuO$ ratio heated in air at 1000°C. Samples made the same way in the composition range $1.5La_2O_3 \cdot 2CuO$ to $1La_2O_3 \cdot 3CuO$, and electron microscope microanalysis, indicated that the composition of the new phase was very close to $La_1Cu_1O_x$. The complexity of the powder X-ray diffraction pattern indicated that the crystallographic unit cell was large, and so a single crystal structure analysis was necessary to determine the exact La : Cu ratio in the new compound.

Small single crystals of $La_2Cu_2O_5$ were grown by heating a mixture of 1CuO and $1LaCuO_x$ (prepared at 1000°C in air) in an Al_2O_3 crucible in air to 1040°C. After holding at 1040°C for 10 hr, the partially melted material was cooled at 1°/hr to 1015°C and then pulled from the furnace. The product was a mixture of CuO, Cu_2O, La_2CuO_4, and the new phase. Crystals of the new phase were picked out through EDX analysis on a scanning electron microscope.

The crystal structure of the compound is described in the subsequent section. The results indicated that the La : Cu ratio was indeed 1 : 1. Single phase material was therefore prepared by making four 1-day heating and grinding cycles of $LaCuO_x$ in air at 1000°C. The oxygen content of the single phase material was determined by heating to 1000°C in 85% N_2–15% H_2 and measuring the weight loss according to

$$LaCuO_x \rightarrow 0.5La_2O_3 + 1Cu + 0.5(x - 1.5)O_2$$

The resulting oxygen content yielded a formula of $La_2Cu_2O_5$ to within the experimental precision of ± 0.02, and therefore a formal copper valence of $+2$. Heating of the single phase material at 5°/min in O_2 to 1000°C did not result in weight gain or loss. Heating in N_2 showed a weight loss corresponding to decomposition at 800°C. Therefore, it appears that the range of oxygen stoichiometry for $La_2Cu_2O_5$ at near ambient conditions is very small.

$La_2Cu_2O_5$ appears to be either metastable or only slightly more stable than a 1 : 1 mixture of La_2CuO_4 and CuO. If $0.5La_2O_3 + 1$ CuO are heated at 900°C in air until reaction is complete, the result is $La_2CuO_4 + CuO$. If that material is then heated at 1000°C in air for periods of several days the phase assemblage is unchanged. To the detectability limit of powder X-ray diffraction, *no* $La_2Cu_2O_5$ is formed. Thus successful synthesis of the phase requires fast heating into the temperature stability region to prevent the formation of La_2CuO_4, achieved in our case by direct insertion of the La_2O_3–CuO mixture into a hot furnace.

To determine the temperature range in which $La_2Cu_2O_5$ can be synthesized, samples of $0.5La_2O_3 + CuO$ powders, (in Al_2O_3 crucibles) mixed as described, were inserted into a gradient furnace spanning the temper-

TABLE I

STABILITY OF $La_2Cu_2O_5$

Atmosphere: Air
Input: La_2O_3 + 2CuO

Temperature (°C)	Status	Major Phase(s)
1038	Part melt	La_2CuO_4 + CuO
1035	Part melt	La_2CuO_4 + CuO
1030	Part melt	La_2CuO_4 + CuO
1025	Part melt	$La_2Cu_2O_5$
1020	Part melt	$La_2Cu_2O_5$
1018	Part melt	$La_2Cu_2O_5$
1012	No melt	$La_2Cu_2O_5$
1006	No melt	$La_2Cu_2O_5$
999	No melt	$La_2Cu_2O_5$
985	No melt	$La_2Cu_2O_5$ + $La_8Cu_7O_{19}$
968	No melt	La_2CuO_4 + CuO
950	No melt	La_2CuO_4 + CuO

ature range of 950–1038°C, in an air ambient. Heating time was 4 days. Samples were pulled out of the furnace hot. The results are presented in Table I. Major phases observed by X-ray diffraction are presented as well as the melt/no-melt status determined by visual inspection. Single-phase $La_2Cu_2O_5$ is formed only in the 13°C temperature range between 999 and 1012°C. Between 1018 and 1025°C, $La_2Cu_2O_5$ is in equilibrium with a liquid eutectic. This information was used to design the crystal growth experiment. Above 1025°C and below 985°C, $La_2Cu_2O_5$ is no longer found even as part of a multiphase mixture. These very narrow stability ranges, as well as the poor stability with respect to La_2CuO_4 + CuO, are no doubt what has made this phase so elusive.

The sample heated at 985°C was a two-phase mixture of $La_2Cu_2O_5$ with an additional unknown phase whose powder pattern appeared to be related to that of $La_2Cu_2O_5$. After determination of the crystal structure of $La_2Cu_2O_5$ and analysis of the high resolution lattice images, we realized

TABLE II

STABILITY OF $La_8Cu_7O_{19}$

Atmosphere: O_2
Input: Prereacted $La_8Cu_7O_{19}$

Temperature (°C)	Status	Major Phase(s)
1061	Full melt	La_2CuO_4 + CuO
1058	Part melt	La_2CuO_4 + CuO
1054	Part melt	$La_2Cu_2O_5$ + La_2CuO_4
1050	No melt	$La_2Cu_2O_5$ + $La_8Cu_7O_{19}$
1044	No melt	$La_8Cu_7O_{19}$ + small $La_2Cu_2O_5$
1037	No melt	$La_8Cu_7O_{19}$
1030	No melt	$La_8Cu_7O_{19}$
1019	No melt	$La_8Cu_7O_{19}$
1006	No melt	$La_8Cu_7O_{19}$ + La_2CuO_4
990	No melt	$La_8Cu_7O_{19}$ + La_2CuO_4
950–850	No melt	La_2CuO_4 increases as temperature decreases

TABLE III

DATA COLLECTION PARAMETERS OF $La_2Cu_2O_5$

Space group	$C\,2/c$ (unique axis b)
a (23.2°C)	13.8640(14) Å
b	3.7469(3) Å
c	27.943(3) Å
β	106.06(2)°
Volume	1394.91(22) Å
Z	12
Calculated density	6.93 g/cm^3
Absorption coefficient μ	150.9 mm^{-1}
Crystal size	0.05 × 0.04 × 0.12 mm^3
Min. transm.	0.0019
Max. transm.	0.4198
Scan mode	$\omega - 2\theta$
$2\theta_{max}$	150°
Measured reflections	5226
Unique reflections	1431
Observed reflections ($I_{net} > 2.5\sigma(I)$)	1291
Parameters	86
R_f (obs)	0.069
R_f (all)	0.074
R_w (obs)	0.072
R_w (all)	0.075
Extinction length	0.81(7) μm

Note. ESD's are given in parentheses.

that this might be another phase in a homologous series of the type $La_{4+4n}Cu_{8+2n}O_{14+8n}$, where $La_2Cu_2O_5$ is the $n = 2$ member. We therefore attempted to synthesize the $n = 3$ member, $La_8Cu_7O_{19}$, in an analogous manner. Because it apparently could not be made as a single phase easily in air, we explored its synthesis in O_2. Preliminary experiments indicated that the phase mixed with $La_2Cu_2O_5$ in air at 985°C could be made single phase to X-ray diffraction at 1020°C in O_2. Starting with $La_8Cu_7O_{19}$, reacted as described for $La_2Cu_2O_5$, but at 1020°C in O_2 for 2 days, powders were placed in Al_2O_3 crucibles and fired in O_2 for 3 days in gradient furnaces in the temperature range 850–1061°C to determine the temperature stability region of the phase. The results are presented in Table II. $La_8Cu_7O_{19}$ can be made single phase only in the 18°C interval 1019–1037°C. On heating at 1044 and above, first $La_2Cu_2O_5$ appears mixed with $La_8Cu_7O_{19}$ as a solid phase. There is a partial melting region near 1054 where $La_2Cu_2O_5$ and La_2CuO_4 are found, but there is *no* temperature interval where $La_8Cu_7O_{19}$ is found in equilibrium with a melt. This suggests that simple slow cooling of a La_2O_3–CuO melt might not be sufficient to produce crystals of this phase.

TABLE IV

ATOM POSITIONS OF $La_2Cu_2O_5$

Atom	Position	x	y	z	B_{iso} (Å^2)
La 1	8*f*	0.6184(1)	−0.0196(4)	0.2317(1)	0.52(6)
La 2	8*f*	0.2326(1)	−0.0335(4)	0.1350(1)	0.52(7)
La 3	8*f*	0.4719(1)	0.0072(4)	0.0983(1)	0.54(6)
Cu 1	8*f*	0.0765(3)	0.015(1)	0.8192(2)	0.71(17)
Cu 2	8*f*	0.2242(3)	0.005(1)	0.4609(2)	0.78(17)
Cu 3	8*f*	0.0932(3)	0.122(1)	0.0288(2)	0.80(17)
O 1	4*e*	0	−0.012(8)	0.25	0.5(4)
O 2	8*f*	0.849(2)	−0.004(6)	0.1106(7)	0.7(3)
O 3	8*f*	0.923(2)	0.480(6)	0.1810(7)	0.6(3)
O 4	8*f*	0.245(2)	0.010(6)	0.0349(7)	0.7(3)
O 5	8*f*	0.272(2)	0.472(6)	0.2083(7)	0.7(3)
O 6	8*f*	0.131(2)	0.444(6)	0.0845(8)	0.8(3)
O 7	8*f*	0.961(2)	0.019(6)	0.0379(8)	0.9(3)
O 8	8*f*	0.584(2)	0.461(6)	0.1615(8)	0.9(3)

Note. ESD's are given in parentheses.

TABLE V

INTERATOMIC DISTANCES IN $La_2Cu_2O_5$

La 1	—	O 1	2.61(2)	La 2	—	O 2	2.60(2)
	—	O 1	2.65(2)		—	O 2	2.76(2)
	—	O 3	2.65(2)		—	O 3	2.59(2)
	—	O 3	2.69(2)		—	O 4	2.85(2)
	—	O 5	2.40(2)		—	O 5	2.70(2)
	—	O 5	2.67(2)		—	O 5	2.73(2)
	—	O 5	2.71(2)		—	O 6	2.46(2)
	—	O 8	2.61(2)		—	O 6	2.59(2)
	—	O 8	2.71(2)		—	O 8	2.38(2)
La 3	—	O 2	2.59(2)	Cu 1	—	O 1	1.93(2)
	—	O 2	2.65(2)		—	O 2	1.95(2)
	—	O 3	2.59(2)		—	O 3	1.86(2)
	—	O 4	3.16(2)		—	O 3	1.89(2)
	—	O 6	2.36(2)		—	O 5	2.43(2)
	—	O 7	2.46(2)		—	O 8	2.43(2)
	—	O 7	2.53(2)				
	—	O 8	2.62(2)				
	—	O 8	2.86(2)				
Cu 2	—	O 2	1.97(2)	Cu 3	—	O 4	2.10(2)
	—	O 4	1.90(2)		—	O 6	1.92(2)
	—	O 4	1.94(2)		—	O 7	1.88(2)
	—	O 4	2.01(2)		—	O 7	1.96(2)

Note. ESD's are given in parentheses.

Crystal Structure of $La_2Cu_2O_5$

Electron diffraction patterns indicated that $La_2Cu_2O_5$ had a monoclinic symmetry *C*-centered unit cell of approximate dimension 13.8 × 3.75 × 28 Å, $\beta \approx 106°$. The 28-Å *c* axis was due to a weak superlattice, doubling the strong subcell reflections for a *c* axis of approximately 14 Å. A single crystal of $La_2Cu_2O_5$ was mounted on a CAD-4 diffractometer (graphite monochromatized Cu$K\alpha$ radiation) controlled by the NRCCAD program. At first, a monoclinic unit cell with $a = 13.865$, $b = 3.747$, $c = 13.972$, and $\beta = 106.07°$, space group $C2/m$ was found. Data was collected for this unit cell, and a structure refinement was attempted. The result clearly indicated that a superstructure had to be present, since one copper atom showed up in a position with half occupation and a short copper–copper distance of 0.6 Å. Further X-ray examina-

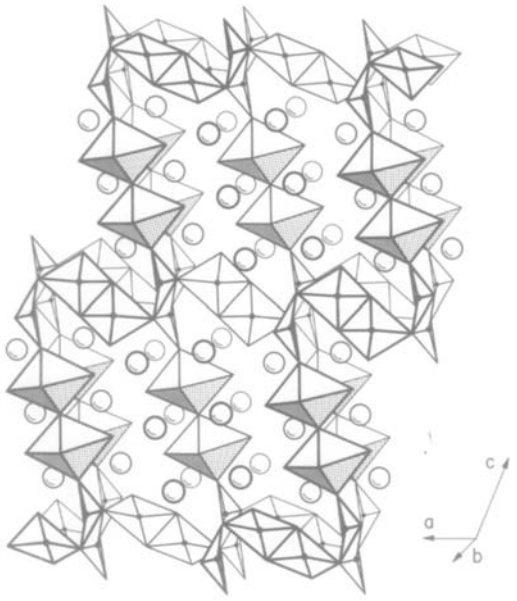

FIG. 1. The crystal structure of $La_2Cu_2O_5$. The large open circles are La, and the Cu–O coordination polyhedra are outlined. Small closed circles are Cu four-coordinated with oxygen.

tion of the crystal confirmed the TEM diffraction patterns on powder samples, indicating a doubling of the unit cell along the c axis, with possible loss of the C-centering. Another set of data based on the new full unit cell was then collected. The data collection parameters are given in Table III. Unit cell parameters were obtained by determining the absolute 2θ values ($CuK\alpha_1$) of 34 reflections in the range of 80° to 90° and

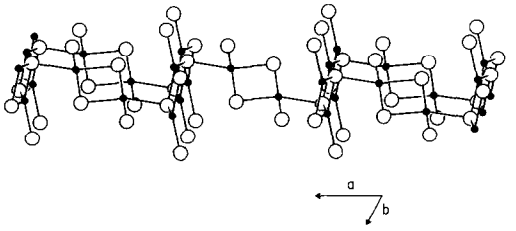

FIG. 2. Detail of the Cu–O bonding scheme in the complex Cu–O planes. Large circles, oxygen; small solid circles, copper. Note the puckered CuO double chains running parallel to b.

TABLE VI

POWDER DIFFRACTION PATTERN FOR $La_2Cu_2O_5$

$CuK\alpha_1$ radiation, $C2/c$
a = 13.869(3), b = 3.7487(5), c = 27.967(5),
β = 106.06(1)

				2θ	
h	k	l	I/I_0	Observed	Calculated
0	0	2	2	6.57	6.57
0	0	4	4	13.14	13.17
0	0	6	4	19.80	19.80
1	1	0	8	24.66	24.65
1	1	−2	14	25.05	25.04
4	0	−4	20	26.34	26.34
2	0	6	16	26.85	26.86
4	0	−6	13	28.62	28.60
4	0	2	28	29.34	29.32
3	1	−2	27	30.69	30.70
3	1	0	4	31.22	31.19
3	1	−4	63	31.65	31.66
2	0	−10	51	32.23	32.26
1	1	6	100	33.00	32.99
3	1	−6	3	33.99	33.97
4	0	−10	5	36.68	36.66
1	1	8	18	37.92	37.90
6	0	−4	4	38.97	38.99
6	0	−6	33	39.99	39.97
1	1	−10	7	40.29	40.28
6	0	0	21	40.56	40.58
5	1	−6	32	41.87	41.89
4	0	−12		41.87	41.88
6	0	2	5	43.04	43.03
5	1	2	27	43.64	43.64
3	1	8	3	45.05	45.06
2	0	12	36	46.16	46.15
3	1	−12	16	46.76	46.77
0	0	14	6	47.30	47.31
0	2	0	34	48.56	48.53
0	2	2	4	49.01	49.03
1	1	12	3	49.40	49.43
2	2	−2	4	50.48	50.48
5	1	−12	5	51.56	51.54
2	0	14	16	53.15	53.13
7	1	0	17	53.97	53.97
7	1	−8	27	54.16	54.14
5	1	8	10	55.24	55.24
8	0	−10	21	56.30	56.30
4	2	2	13	57.70	57.71
1	1	−16	9	58.83	58.82

applying a least-squares refinement. The previously solved substructure served as the starting model for the superstructure re-

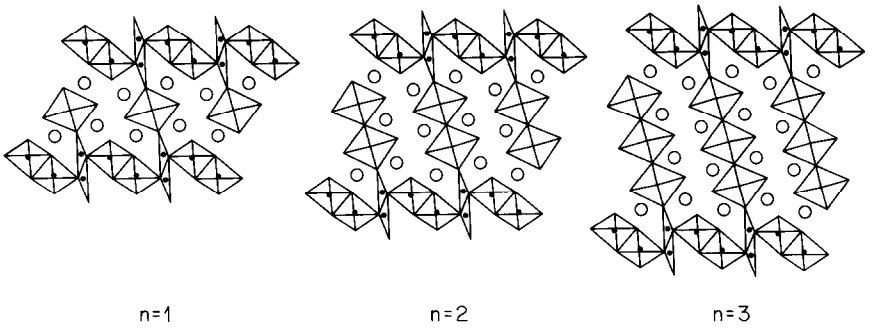

FIG. 3. The homologous series principle for $La_{4+4n}Cu_{8+2n}O_{14+8n}$ for the basic structural unit (subcell). $La_2Cu_2O_5$ and $La_8Cu_7O_{19}$ are the $n = 2$ and $n = 3$ members, where n is the number of octahedra in the width of the La_2CuO_4 type block.

finement, which converged immediately. Atomic positions are given in Table IV and interatomic distances in Table V.

The crystal structure of $La_2Cu_2O_5$ is shown in Fig. 1. The complexity of the structure is remarkable considering the simple ratio of component elements. The structure consists of thin, skew planes of La_2CuO_4 sandwiched between planes made of edge-shared copper–oxygen coordination polyhedra with highly distorted geometries. The La_2CuO_4 planes are *not* those which are usually observed as building blocks in Ruddlesden–Popper series compounds. Those are 3.9 × 3.9 Å *a–b* plane layers; these are based on La_2CuO_4 layers having the *b* axis in one direction and the [101] axis in the other direction. Remarkably, the Cu–O elongated octahedral geometry and the ninefold La–O-capped square antiprismatic geometry in these layers are virtually identical to those found in La_2CuO_4.

The unique components of the structure of $La_2Cu_2O_5$ are the complex copper–oxygen planes which terminate the La_2CuO_4 planes at a width of two octahedra. One of these Cu–O planes is shown in detail in Fig. 2. It consists of two structural subunits. The first subunit is a double Cu–O chain running parallel to the *b* axis, very similar to the double chain found in $YBa_2Cu_4O_8$. In $La_2Cu_2O_5$, however, the CuO diamonds in the double chain are puckered to the degree of being flattened tetrahedra. These double chains bond directly to the corners of the octahedra in the La_2CuO_4 type planes. The second subunit, between the double chains, is pairs of distorted CuO_4 tetrahedra sharing a common edge, and sharing corners with the double chains. The copper atoms in these tetrahedra are positionally ordered along *b* as one goes from one of the complex planes shown in Fig. 2 to the next one on the opposite side of the truncated La_2CuO_4 planes, *c*/2 away. This is the origin of the superlattice. As can be seen by inspection of the atomic coordinates in Table IV, the remainder of the atoms distort slightly from their ideal (subcell) positions of $y = 0.0$ or 0.5 to accommodate the ordering. Referring back to Fig. 1, which shows one supercell with $c = 27.9$ Å, the strong subcell is apparent with a *c* axis of (27.9)/2 Å: the La_2CuO_4 type structural component and most of the complex Cu–O plane are conserved as one moves from the upper to the lower structural unit; only the positions of the tetrahedra in the complex planes has changed.

Lanthanum–oxygen and copper–oxygen bond lengths are presented for $La_2Cu_2O_5$ in

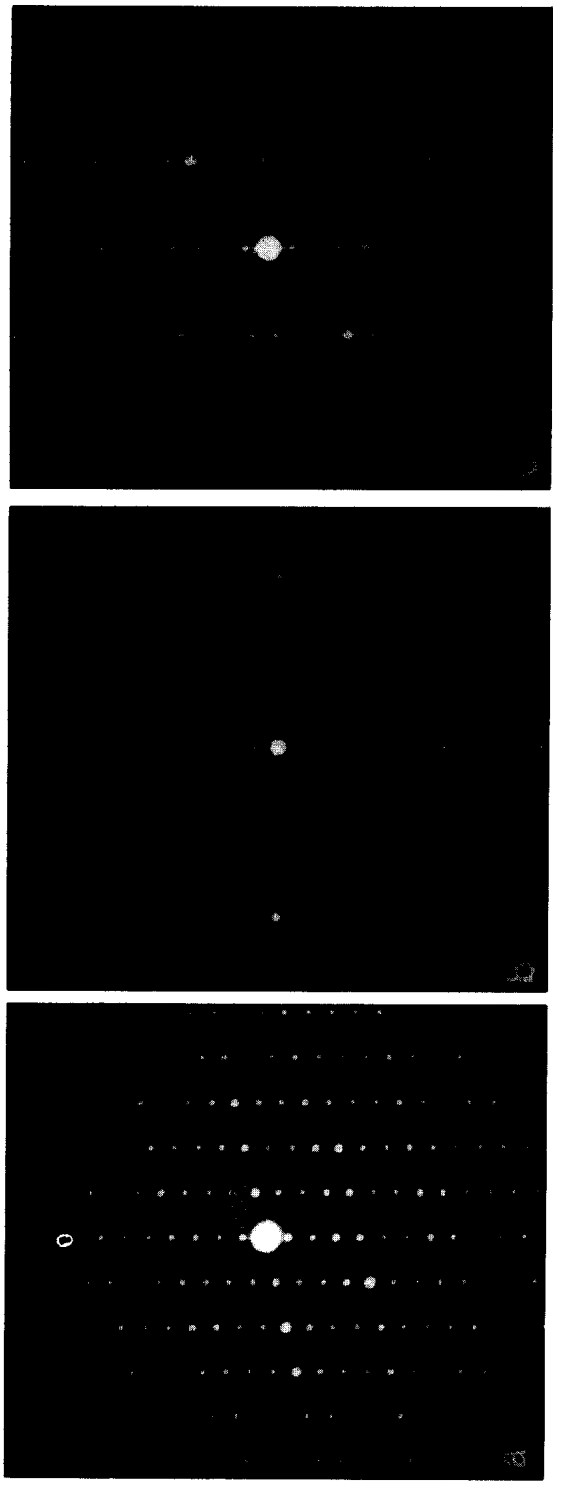

FIG. 4. Series of electron diffraction patterns tilted about the c^* axis: (a) along a^* (b) along b^* and (c) along $[\bar{1}\bar{4}10]$. (a) and (b) show only a little streaking along c^*. Taken from a thick crystal, (c) shows strong reflections hkl with $l = 2n + 1$ and streaking along c^*.

TABLE VII

POWDER DIFFRACTION PATTERN FOR $La_8Cu_7O_{19}$

$CuK\alpha_1$ radiation
a = 13.84(1), b = 3.756(1), c = 34.64(1),
β = 98.99(7)

				2θ	
h	k	l	I/I_0	Observed	Calculated
0	0	4	2	10.35	10.33
2	0	−2	5	13.15	13.16
2	0	−4	2	15.27	15.26
0	0	6	3	15.51	15.53
0	0	8	3	20.80	20.76
1	1	0	11	24.58	24.56
1	1	−2	15	24.90	24.89
2	0	8	8	26.15	26.23
4	0	−4	24	26.47	26.50
2	0	−10	4	27.25	27.24
4	0	−6	6	28.20	28.24
1	1	6	28	29.73	29.74
3	1	−2	28	30.75	30.74
3	1	−4	69	31.55	31.56
2	0	−12	36	32.05	32.04
1	1	8	100	33.10	33.04
1	1	10	9	36.90	36.85
4	0	−12	3	37.75	37.76
1	1	−12	3	39.33	39.37
6	0	−6	20	40.20	40.22
5	1	−4	13	40.83	40.81
5	1	−6	34	41.85	41.88
5	1	−8	24	43.62	43.61
3	1	−14	12	46.08	46.10
0	2	0	32	48.40	48.42

Table V. The lanthanum–oxygen and octahedral copper (Cu1)–oxygen bond lengths are very similar to those found in La_2CuO_4 (*8*). Note especially that the Jahn–Teller distortion of the copper–oxygen octahedron in $La_2Cu_2O_5$, with four in-plane distances near 1.9 Å and two apical oxygen bond lengths near 2.4 Å, is virtually identical to that in La_2CuO_4. The four-coordinated copper (Cu2) in the puckered double chains displays Cu–O bond lengths near 1.95 Å, as does the tetrahedral copper (Cu3) between the chains.

Due to the low symmetry and large unit cell of $La_2Cu_2O_5$, the powder X-ray diffraction pattern consists of many lines. The indexed diffraction pattern for $CuK\alpha$ radiation for material prepared at 1006°C in air is presented in Table VI. The refined crystallographic cell parameters (Cu_2O internal standard) are a = 13.869(3), b = 3.7487(5), c = 27.967(5), β = 106.06(1)°. Note that only reflections with l = even are observed, indicating the dominance of the $c/2$ subcell in determining the powder X-ray diffraction intensities.

The Homologous Series

Inspection of the crystal structure of $La_2Cu_2O_5$ suggests a structural building principle for a series of compounds of similar structure. In this series, the width of the La_2CuO_4 type layer inserted between the complex Cu–O planes is variable between

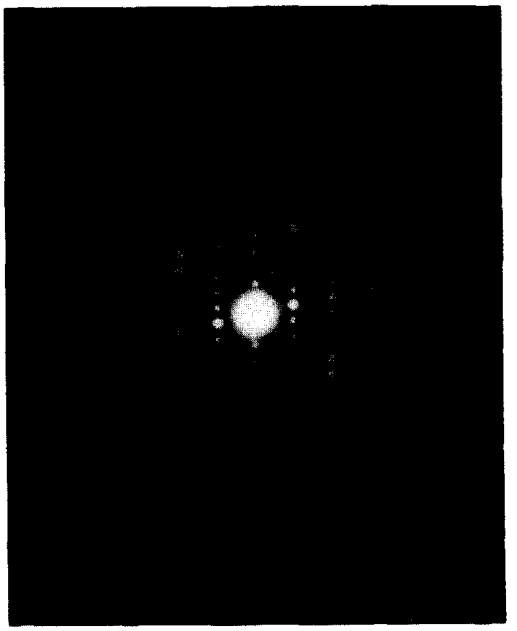

FIG. 5. An [010] electron diffraction pattern of $La_8Cu_7O_{19}$. No streaking along c^* can be observed, indicating the absence of stacking faults.

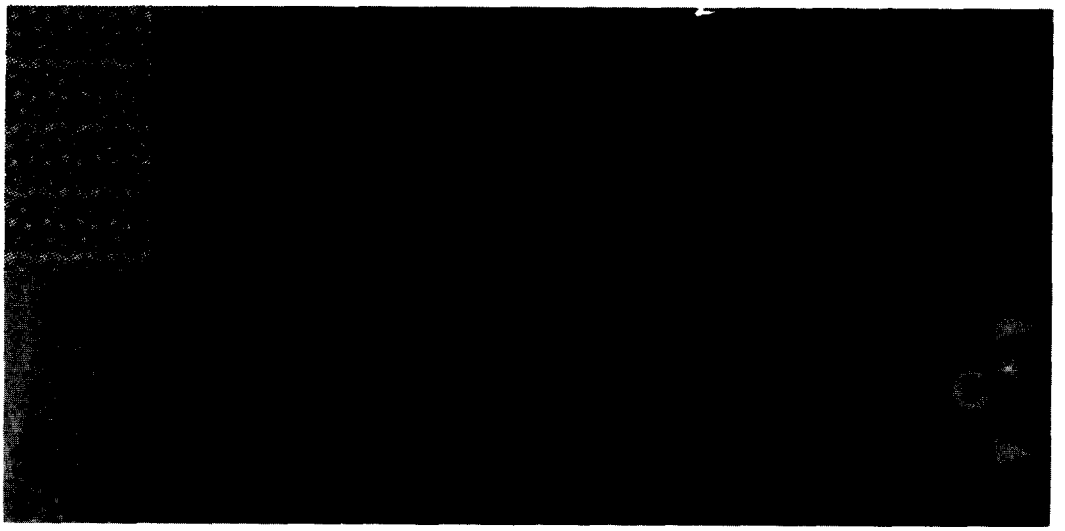

FIG. 6. HREM image along the *b* axis showing a structure image of $La_2Cu_2O_5$. La ions are imaged as dominant white dots. The inset shows a calculated image for which the parameter defocus = −105 nm, Cs = 2.0 mm, defocus spread = 8 nm, objective aperture = 5 nm^{-1}, and convergence angle = 0.7 mrad are used.

one octahedron and an infinite number of octahedra (pure La_2CuO_4). As the number of octahedra between the Cu–O planes increases, the stability of any member of the series with respect to a mixture of pure La_2CuO_4 plus a $La_2Cu_2O_5$ type compound with a smaller layer width decreases. For the case of the two-octahedra-wide compound, $La_2Cu_2O_5$, the stability range in temperature is already very narrow. Thus, members with wider La_2CuO_4 blocks are not likely to be easily synthesized.

Inspection of the lattice images obtained by electron microscopy, described in a subsequent section, indicated that in defective regions in $La_2Cu_2O_5$, different width La_2CuO_4 type blocks were indeed observed, intergrown with the two-octahedra blocks. The formula for the new homologous series, deduced by analysis of the structure of $La_2Cu_2O_5$, is $La_{4+4n}Cu_{8+2n}O_{14+8n}$, n = 1, 2, 3 . . . , where n is the number of CuO_6 octahedra in the width of the La_2CuO_4 blocks. We write the formula normalized to the number of atoms in the crystallographic subcell. $La_2Cu_2O_5$ is the n = 2 member. A schematic representation of the first three members of the series is presented in Fig. 3.

Our attempts to synthesize the n = 1 member, $La_4Cu_5O_{11}$, were not successful. For $La_8Cu_7O_{19}$, synthesized as described, electron microscope lattice images indicated predominantly the n = 3 structure, intergrown with some n = 2 and n = 4. The powder X-ray diffraction pattern, while very similar to that of $La_2Cu_2O_5$, is nonetheless distinctly different in detail. Based on the unit cell determined by electron diffraction, the powder pattern was indexed and the cell constants determined. The material is monoclinic, C-centered, with a = 13.84(1), b = 3.756(1), c = 34.64(1), β = 98.99(7)°, in excellent agreement with what is expected based on the cell size estimated from analysis of Fig. 3. The powder pattern (Cu$K\alpha_1$ radiation) for $La_8Cu_7O_{19}$ is presented in Table VI. A shoulder on the largest peak, with $I/I_0 \sim 15\%\ I_{max}$, at 2θ = 32.73°,

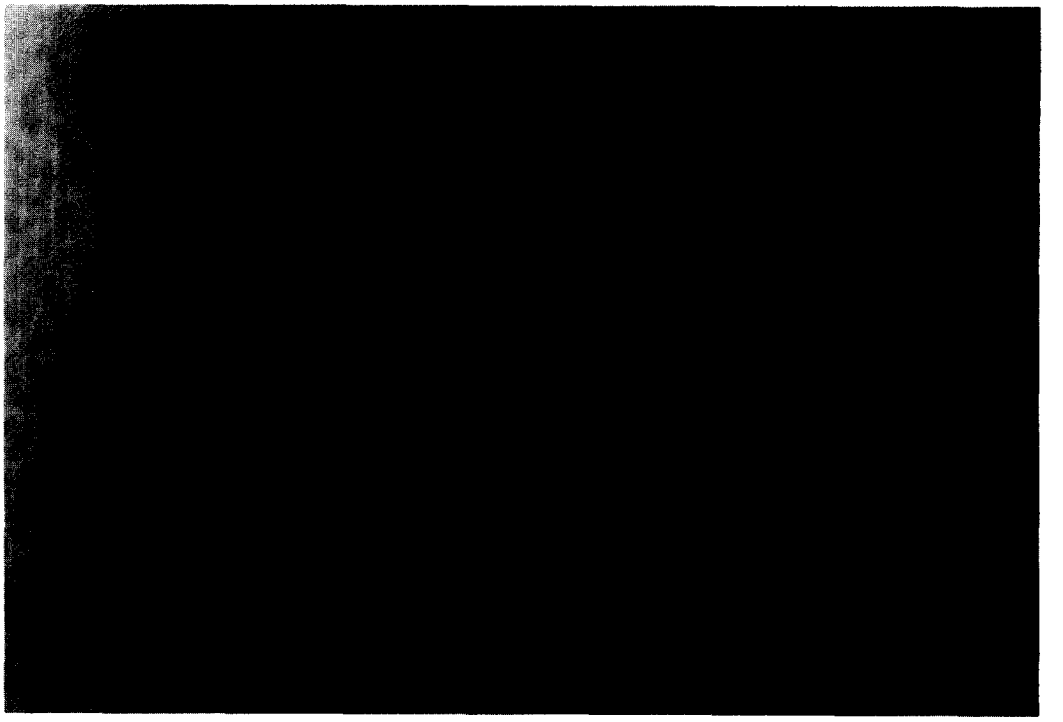

FIG. 7. HREM image of $La_2Cu_2O_5$ along $[\bar{1}410]$ showing regions in which the supercell periodicity along the c axis is absent. The supercell (27.9 Å) periodicity is only visible in the thicker regions because multiple scattering increases the intensities of the hkl reflections with $l = 2n + 1$. Periodicity is indicated with arrows.

could not be indexed on this cell or that of any other known compounds, suggesting either that the symmetry of $La_8Cu_7O_{19}$ may actually be lower than monoclinic, or that another member of the series other than $n = 2$ or 3 may be present.

Electron microscope lattice images of $La_8Cu_7O_{19}$ revealed the presence of regions of the $n = 4$ member of the homologous series, $La_{10}Cu_8O_{23}$. We therefore attempted to synthesize that material as a bulk phase directly from $La_2O_3 + CuO$ by heating in O_2 for 5 days, between 950 and 1050°C, at 10° intervals. Powder X-ray diffraction analysis revealed that the materials were in all cases mixtures of La_2CuO_4, $La_2Cu_2O_5$, and $La_8Cu_7O_{19}$ (including the unindexed peak).

Electron Microscopy

Thin specimens for electron microscopy were prepared in two ways. First, by grinding and mounting on a carbon-coated holey film supported by a Cu grid. Second, by Ar ion milling 20-μm thin pellets, obtained by pressing ground material, starting with a 20° incidence angle, 5 kV, and 2 μA, and finishing after a hole was obtained with 12°, 3 kV, and 1 μA for 45 min; all ion milling was performed with liquid nitrogen cooling of the specimen. Electron microscopy was performed with a Philips CM30T electron microscope, operating at 300 kV, equipped with a side-entry 60°/30° tilt specimen holder, and a Link EDX detector.

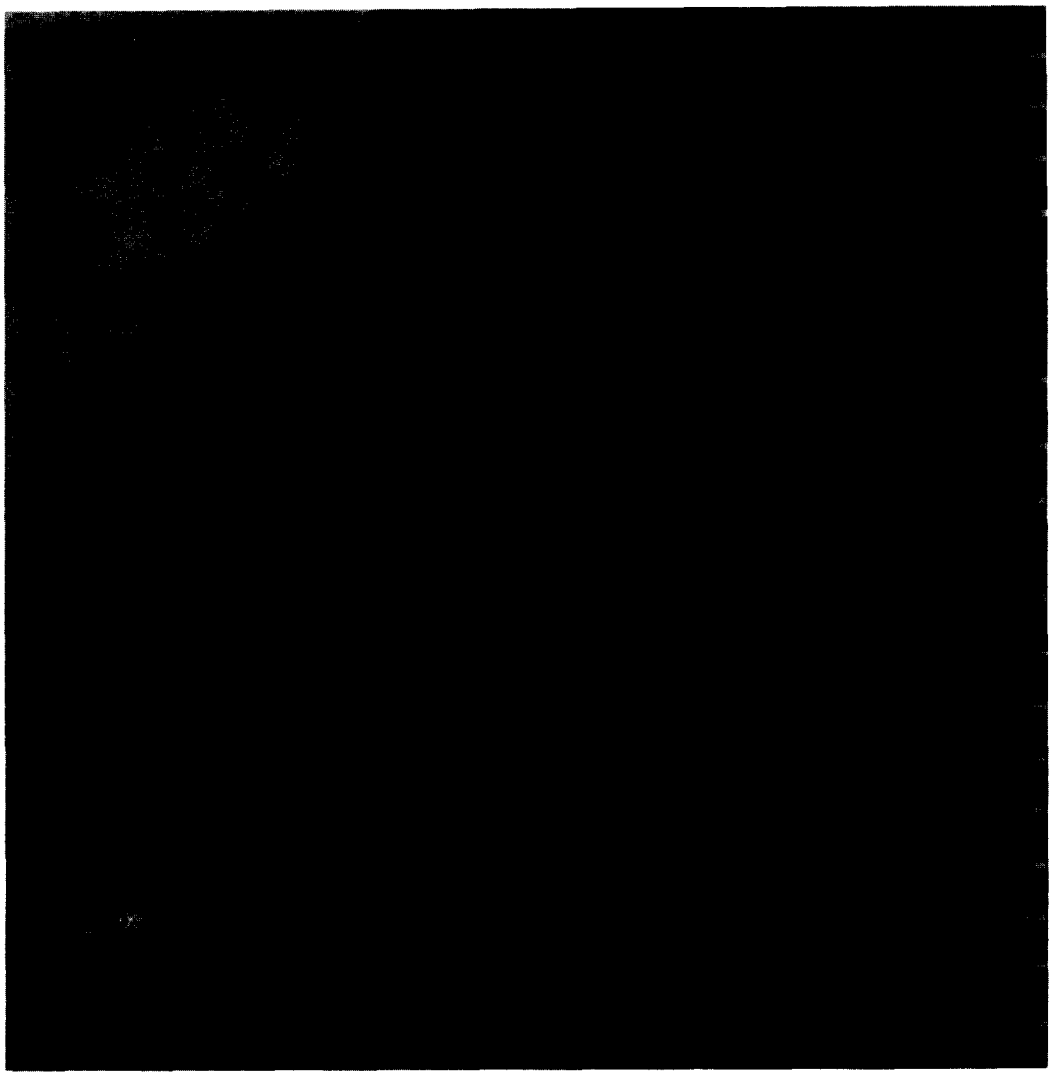

FIG. 8. HREM image along [$\bar{1}$410] showing stacking defects corresponding to the $n = 3$, $n = 5$, and $n = 10$ members of the homologous series $La_{4+4n}Cu_{8+2n}O_{14+8n}$. This projection shows n rows of dominant white dots between complex Cu–O planes. The arrows indicate the periodicity $c^*/2$.

Electron diffraction results on $La_2Cu_2O_5$ powders prepared in air at 1000°C were consistent with a unit cell of $a = 13.9$, $b = 3.7$, $c = 27.9$ Å, $\gamma = 106°$ and C type Bravais lattice (see Fig. 4). The reciprocal lattice was scanned by rotating about the c^* axis. The hkl reflections with $l = 2n + 1$ are only strong for thick crystals, indicating that these reflections are quite weak. These reflections can become strong for thicker regions due to multiple scattering. A small number of crystallites did not exhibit a c axis of 27.9 Å but only the subcell period of $c/2$. A relatively high number of crystallites

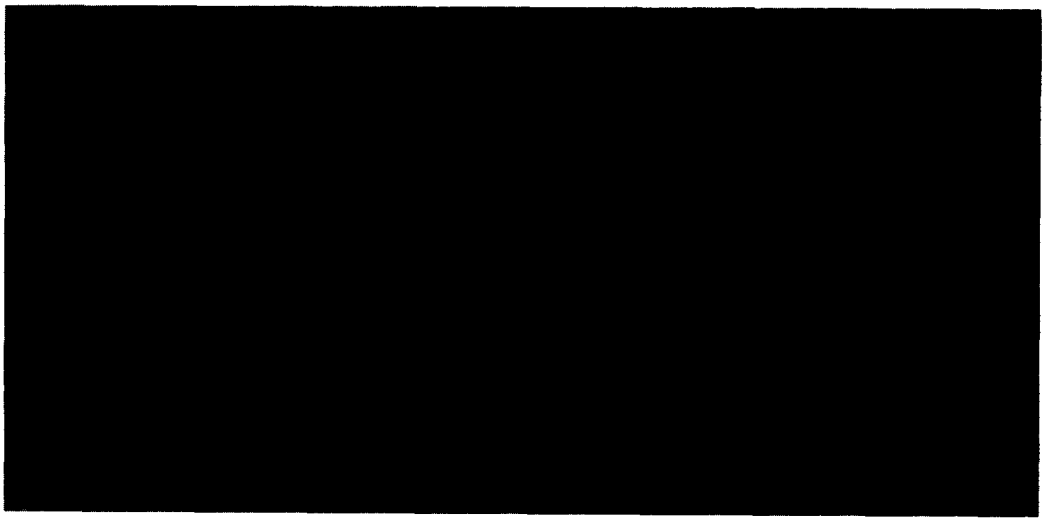

FIG. 9. HREM image along the b axis of $La_8Cu_7O_{19}$. La ions are imaged as dominant white dots.

showed streaking along the c^* direction. The degree of streaking varied from region to region. The streaking indicates that planar defects, due to intergrowth of regions of different n, occur in the c^* direction. These results are in agreement with high resolution electron microscopy (HREM), which showed the presence such stacking faults. In a number of crystals, streaking is also observed along c^* through the forbidden $0hl$ reflections with $h = 2n + 1$. This streaking might also be caused by the same intergrowth.

Electron diffraction results on $La_8Cu_7O_{19}$ showed the material to have a monoclinic unit cell of $a \cong 13.9$, $b \cong 3.7$, $c \cong 35.0$ Å and $\beta \cong 100°$, and a C type of Bravais lattice. As for $La_2Cu_2O_5$ there is a strong $c/2$ subcell reflecting the basic structural unit. The powder diffraction pattern (Table VII) has been indexed on the $c \cong 35$ Å cell based on the electron diffraction results: only the subcell reflections are visible in the X-ray data. A large variation was observed in the amount of streaking along c^* for $La_8Cu_7O_{19}$, reflecting the presence of other phases in the homologous series. An example of the [010] diffraction pattern for pure $La_8Cu_7O_{19}$ is shown in Fig. 5.

HREM was carried out on crystals of $La_2Cu_2O_5$ and $La_8Cu_7O_{19}$ along b^*, containing the [100] and [001] directions, and along $[\bar{1}401]$, containing the [110] and [001] directions. For the homologous series $La_{4+4n}Cu_{8+2n}O_{14+8n}$, where n = the number of CuO_6 octahedra in the width of the La_2CuO_4 blocks, the HREM images along b^* [010] show $(n + 1)$ rows of white dots along c^*, whereas the HREM images a long $[\bar{1}410]$ show (n) rows of white dots along c^*, due to the different kinds of electron scattering conditions. Most crystals of $La_2Cu_2O_5$ showed no or very few defects. An example of an [010] high resolution image is given in Fig. 6. In this image the La ions are imaged as dominant white dots. The image agrees very well with the calculated (from the X-ray structure) image which is shown as an inset in Fig. 6. For other defocus values the agreement between calculated and observed images ia also good. The 27.9-Å c axis periodicity is visible only in the thick regions of $[\bar{1}410]$ images in agreement with electron diffraction results. Since the

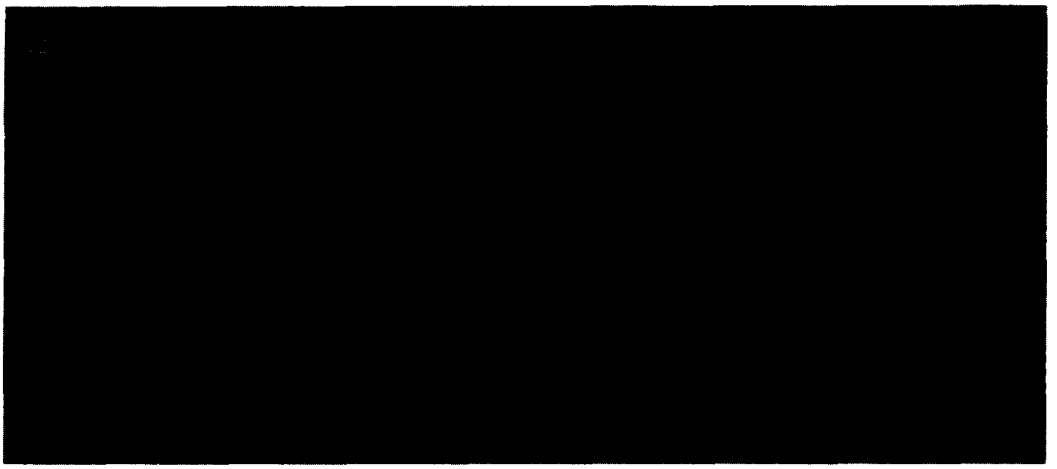

FIG. 10. HREM image along [$\bar{1}4\bar{1}0$] showing the dominance of the $n = 4$ member of the series in this crystal. The $n = 4$ phase existed over a much larger area than is shown in this figure. This projection shows n rows of dominant white dots between complex Cu–O planes.

hkl reflections with $l = 2n + 1$ are weak (the superlattice reflections), one only expects to see this period in the thicker regions, because the intensities of the superlattice reflections can be increased strongly due to multiple scattering of the incident electrons. The 27.9-Å superlattice periodicity is sometimes absent, as can be seen in Fig. 7.

Stacking defects corresponding to various members of the homologous series can often be observed. In Fig. 8, stacking defects corresponding to $n = 3$, $n = 5$, and $n = 10$ are shown in $La_2Cu_2O_5$. In $La_2Cu_2O_5$, $n = 3$ and $n = 4$ defects are observed often; higher members of the homologous series are rare, and the $n = 1$ member has never been observed. HREM on $La_8Cu_7O_{19}$ showed that it was indeed the $n = 3$ member of the homologous series as shown schematically in Fig. 3. A [010] high resolution lattice image of $La_8Cu_7O_{19}$ is presented in Fig. 9. Similar to Fig. 6, the dominant white dots represent the La ions. A number of crystals examined consisted predominantly of the $n = 4$ phase ($La_{10}Cu_8O_{23}$), shown in a HREM [$\bar{1}4\bar{1}0$] image in Fig. 10. We were not successful in synthesizing this phase in the bulk.

Electron beam irradiation can lead to a collapse of the structure: viewed along [$\bar{1}4\bar{1}0$], several crystals lost the 27.9-Å periodicity, leading to a much smaller repeat along the c axis of about 4 Å. This phenomenon suggests that under the conditions in the microscope (high vacuum, reducing electron beam, probably heating by the electron beam), the title compound is not very stable. A small fraction of crystals showed a very high density of defects, being partly antiphase boundaries and stacking defects of the type $La_{4+4n}Cu_{8+2n}O_{14+8n}$.

Physical Properties

For all the compounds in the series, copper is in a 2+ valence state. Therefore they can be expected to be poor electrical conductors, and to have a magnetic susceptibility characteristic of some kind of antiferromagnetic spin interaction. The temperature-dependent electrical resistivity between 300 and 110 K of a polycrystalline pellet of $La_2Cu_2O_5$ measured in a four-probe bar geometry with constant current is presented

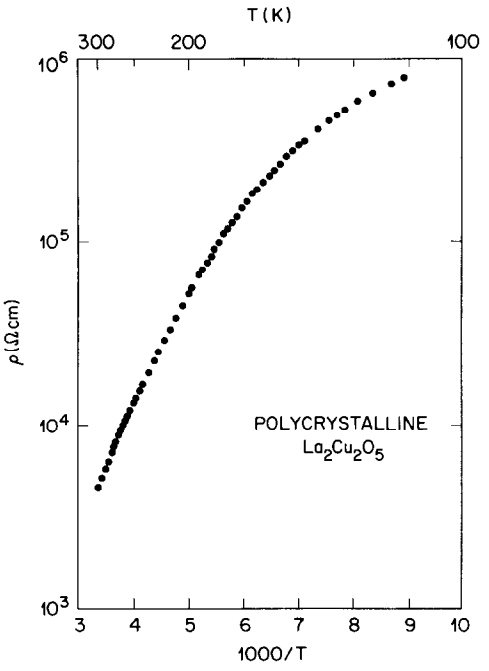

FIG. 11. Temperature-dependent electrical resistivity of polycrystalline $La_2Cu_2O_5$.

in Fig. 11. The resistivity at 300 K is 4.5 × 10^3 ohm cm, and the semiconducting behavior has an activation energy of 0.15 eV near 300 K. The measured behavior no doubt includes the resistivity of ceramic grain boundaries; we expect that the intrinsic single crystal resistivity would be lower.

The magnetic susceptibility of $La_2Cu_2O_5$ and $La_8Cu_7O_{19}$ between 900 and 5 K, measured in a Faraday balance in a field of 10 kOe, is presented in Fig. 12. The most striking observation is the presence of a smooth, broad peak with a full width at half height of nearly 200 K in both materials near 190 K. The shape and width of this peak are very much different from the three-dimensional ordering peaks observed in cuprates, for instance as in La_2CuO_4 (*9*). Rather, the peak is indicative of a low dimensional magnetic ordering with an exchange constant (J) very much smaller than the 1500 K observed for the layered cuprates which are the parent structures of the high T_c compounds. The strength of the exchange constant depends strongly on the colinearity of O–Cu–O and Cu–O–Cu bonding. Inspection of the crystal structures of $La_2Cu_2O_5$ and $La_8Cu_7O_{19}$ indicates that: (a) only the copper atoms in the La_2CuO_4 type slabs have any copper–oxygen colinearity, and that is truncated at a very small number of atoms, and (b) the complex Cu–O planes have a highly distorted copper–oxygen geometry, very far from the 180° bond angles optimal for high exchange constants.

From the peak position, one can estimate J to be approximately 200 K if analyzed in terms of a two-dimensional spin ½ square Heisenberg antiferromagnet, or 300 K for a spin ½ one-dimensional chain antiferomagnet. Because of the complexity of the structure, neither of the two models might be strictly appropriate, but the basic fact that J is very small is unaffected. The origin of this strongly reduced J will have to be found in the details of the O–Cu–O–Cu bonding configuration.

Fits of the susceptibility data in detail to the 2D or 1D Heisenberg model show that the shape of the curves is very close to the ideal form. Only at the highest temperatures

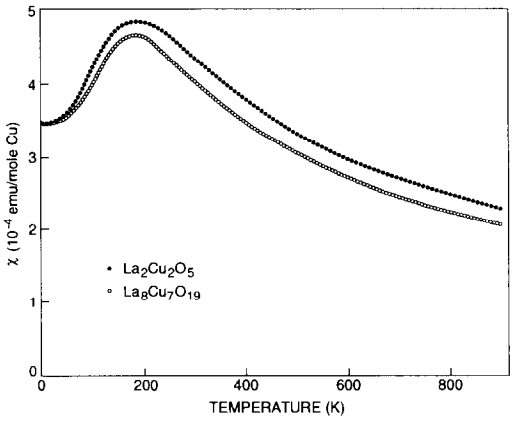

FIG. 12. Temperature-dependent magnetic susceptibilities of $La_2Cu_2O_5$ and $La_8Cu_7O_{19}$.

is there a small, positive deviation. This deviation is indicative of the presence of an additional term in $\chi(T)$ which increases slightly with increasing temperature. We speculate that this part of the susceptibility may be due to the La_2CuO_4 like slabs, with a magnitude strongly reduced from what one might expect, due to the very small size of the slabs. The small size limits the development of the spin correlation length on cooling, and thus the magnitude of the susceptibility. This line of reasoning is supported at least qualitatively by comparison of $\chi(T)$ for $La_2Cu_2O_5$ and $La_8Cu_7O_{19}$ in Fig. 12: if the broad peak in $\chi(T)$ comes from the magnetic behavior of the complex Cu–O planes, then the peak position would be affected only in a minor way or not at all by the number of La_2CuO_4 octahedra, but its fractional contribution to the total susceptibility would decrease with increasing n. This is in fact what is observed.

Summary and Conclusions

We have found that the Ruddelsden–Popper structural series does not occur in the La_2O_3–CuO chemical system under normal synthetic conditions. Rather, a wholly new structural series of formula $La_{4+4n}Cu_{8+2n}O_{14+8n}$ is formed, based on the insertion of skew planes of La_2CuO_4 of different width between complex copper–oxygen planes. The $n = 2$ and $n = 3$ members $La_2Cu_2O_5$ and $La_8Cu_7O_{19}$ can be synthesized as bulk materials, but only in very narrow temperature regions near 1000°C. Although we have not been able to synthesize the $n = 4$ material in bulk form, we often find it intergrown in large areas in $La_8Cu_7O_{19}$. Doping with alkaline earths to introduce holes into the Cu–O array has not been successful in either $La_2Cu_2O_5$ or $La_8Cu_7O_{19}$. These two materials, which contain Cu in its divalent state, have temperature-dependent magnetic susceptibilities characteristic of low dimensional Heisenberg antiferromagnets. Given the simple ratios of the constituent elements, it is remarkable that such complex structures form instead of the simpler Ruddelsden–Popper series. The variety of energetically favorable Cu^{2+}–oxygen coordination polyhedron geometries possible no doubt plays a significant role.

References

1. A. Santoro, F. Beech, M. Marezio, and R. J. Cava, *Physica C* **156,** 693 (1988).
2. D. M. Smyth, *in* "Proceedings of the Superconductor Symposium, 90th Annual Meeting of the American Ceramic Society, Cincinnati, OH, May 1988."
3. S. N. Ruddlesden and P. Popper, *Acta Crystallogr.* **10,** 538 (1957); *Acta Crystallogr.* **11,** 54 (1958).
4. J. F. Bringley, B. A. Scott, S. J. LaPlaca, R. F. Boehme, T. M. Shaw, M. W. McElfresh, and S. S. Trail, *Nature* **347,** 263 (1990).
5. N. Nguyen, L. Er-Rakho, C. Michel, J. Choisinet, and B. Raveau, *Mater. Res. Bull.* **15,** 891 (1980).
6. A. H. Davies and R. J. D. Tilley, *Nature* **326,** 859 (1987).
7. J. B. Torrance, Y. Tokura, and A. Nazzal, *Chemtronics* **2,** 120 (1987).
8. V. B. Grande, H.-K. Muller-Buschbaum, and M. Schweitzer, *Z. Anorg. Allg. Chem.* **428,** 120 (1977).
9. L. F. Schneemeyer, J. V. Waszczak, E. A. Rietman, and R. J. Cava, *Phys. Rev. B* **35,** 8421 (1987).